Recent Advances in Electron-Beam Lithography for the High-Volume Production of VLSI Devices

HANS C. PFEIFFER

Abstract—Recent advances in scanning-electron-beam lithography techniques have increased the efficiency of serial exposure by several orders of magnitude over the basic SEM approach. A spectrum of shaped-beam systems which combine projection and scanning techniques has been developed for various lithographic applications. The first generation of electron-beam production systems at IBM have demonstrated the feasibility of the shaped-beam technique under manufacturing conditions. More advanced shaping techniques such as VSS and Character Projection provide the means to make a high-resolution lithography for VLSI technically and economically feasible.

I. Introduction

ENHANCED productivity is the driving force towards very large-scale integration (VLSI) in the semiconductor industry. The high growth rate for circuit density and the number of circuits per chip is expected to continue for the next five years. Most significant contributions in the past came from improved circuit cleverness and increased chip sizes. However, it is expected that high-resolution lithography will provide the key technology leverage in the near future. Electron-beam exposure tools combined with dry processing (ion implantation, reactive ion etching) can provide the high-resolution lithography required to make VLSI a reality. The superior lithographic capability of electron-beam systems has been thoroughly demonstrated [1]-[9]. The economic feasibility of electron-beam lithography for the mass production of semiconductor devices is not yet clearly demonstrated. So far, industry has not found broad applications for electron-beam direct exposure tools because of their high cost and rather limited exposure speed. The primary application of commercially available systems is mask making, where scanning electron-beam systems compete favorably with optical-mechanical pattern generators. In order to compete with optical alternatives for wafer exposure, the exposure efficiency of electron-beam tools has to be enhanced several orders of magnitude over the basic SEM-type system.

Recent advances in electron-beam lithography which provide the basis for that exposure speed enhancement are the subject of this paper.

II. Imaging Concepts

Electron-beam exposure tools for microlithography are of two basic types: 1) projection systems which expose a high number of image points in parallel; and 2) scanning systems which expose image points serially. Projection systems have potentially high throughput and are less complex than probe-forming scanning systems. The pattern information is inexpensively stored in electron-optical masks. They lack, however, the advantage of pattern generation under computer control and of distortion correction which makes it more difficult to achieve fast and high resolution, registration, and good overlay.

The two most significant projection approaches are 1:1 photocathode projection [10], [11] which typically covers an entire wafer in one exposure and the 10:1 reduction projection [12], [13] which provides the reduced image of a self-supported transparent mask in the target plane. The mask image (3-10 mm) is stepped and repeated over the wafer. A combination of the two projection concepts has been reported as a reduction of a photocathode image [14].

The systems most successfully employed in microlithography, and the primary subject of this paper, are the scanning-electron-beam machines. They combine high spatial resolution with accurate registration and computer-controlled pattern generation as a result of their SEM-like mode of operation. The SEM mode with serial exposure of image points also imposes the most stringent limitations of scanning systems. The exposure rate is typically much lower than that of projection systems—both optical and electron beam. A solution to that problem proved to be the imaging concept of "shaped beams," which combines scanning and projection techniques. The primary application of SEM-type systems is mask making [42] and the direct exposure of some exploratory devices under laboratory conditions. Shaped beams are already established in manufacturing. IBM's EL1 [15] is an example of a shaped-beam manufacturing system for high-volume direct wafer exposure.

III. Shaped Beams

Scanning-electron-beam lithography systems "write" a given pattern area with the focused electron-beam spot under computer control. Fig. 1 shows both the evolution of shaped beams and the exposure advantage the various shaped beams have over the conventional Gaussian round beam.

A. Pattern Generation

The SEM-type Gaussian round beam exposes one image point at a time. The size of the round beam, defined as the half-width of the Gaussian intensity distribution, represents the spatial resolution and is typically 4 or 5 times smaller than the minimum pattern feature. It requires a maximum of 450 beam diameters to expose the I pattern shown.

For shaped-beam systems, the spatial resolution given by the edge slope of the beam profile is decoupled from the

Manuscript received October 10, 1978; revised December 18, 1978.

The author is with IBM Data Systems Division, Hopewell Junction, NY 12533.

This paper is dedicated to Prof. H. Boersch on his 70th birthday.

0018-9383/79/0400-0663$00.75 © 1979 IEEE

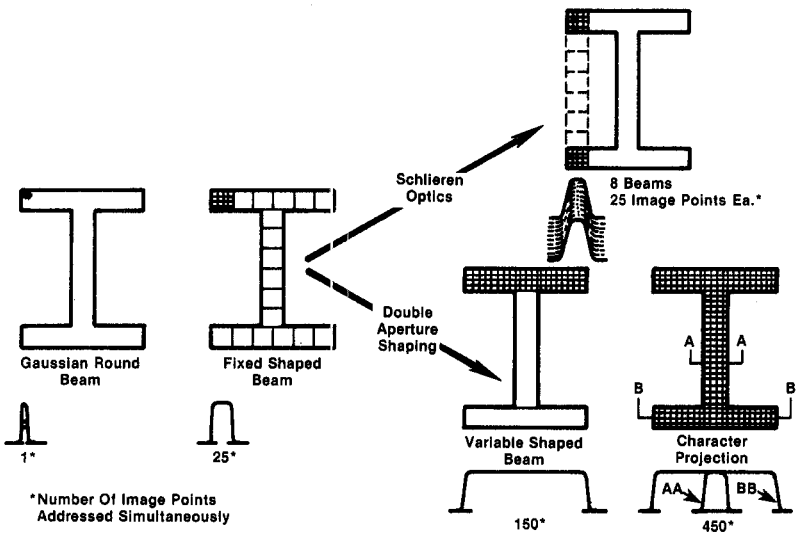

Fig. 1. Pattern generation with various beam profiles. From left to right: the evolution of shaped beams.

size and shape of the beam spot. Consequently, a plurality of image points can be projected in parallel without loss of resolution.

The fixed-shape beam [16], [17] represents the first step in the direction of parallel pattern exposure; 25 image points are projected in parallel. The size of the beam spot is restricted to that of the smallest exposed pattern feature. The parallel projection of a fixed number of image points increases the exposure speed at the price of a certain restriction in pattern flexibility.

To further increase the number of image points projected in parallel, two distinctly different electron optics techniques have been pursued: the "Schlieren" optics multibeam, and the dual-aperture variable-shape beam.

The Schlieren technique [18] produces eight fixed-shape beams in parallel. Projection and deflection of all beams is provided collectively; intensity modulation, however, is applied to each beam individually. The inability to determine the position of each beam on an individual basis represents a limitation for semiconductor applications.

The dual-aperture technique makes beam size and spot shape variable. The variable-shape beam [19] provides a significant increase in throughput over the fixed-shape beam without restricting pattern flexibility. Projected pattern features, however, are still primarily rectilinear. The maximum size of the beam spot is no longer restricted to the minimum pattern feature and up to several hundred image points can be projected in parallel. The shaping variations are performed within 20 ns while the beam steps from one position to the next.

Character projection [20] represents the most advanced beam-shaping technique. Complex pattern cells containing up to 1600 image points (of which 450 are exposed in the example) are addressed and projected in parallel. This technique provides ultimate exposure speed without excessive deflection speed and at a reduced data rate. The technique also overcomes the restriction to rectilinear geometries and is most effective with repetitive patterns.

Next we will describe the various shaping mechanisms.

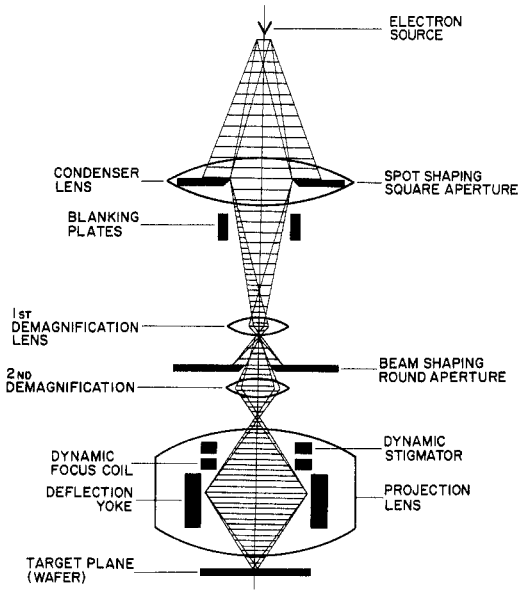

Fig. 2. Fixed-shape-beam imaging concept of ELI.

B. Fixed-Shape Beam

The fixed-shape beam concept is the basis for the more advanced shaping techniques; it gained some attention as the electron-beam approach of IBM's manufacturing system EL1 [15].

Fig. 2 shows the basic imaging concept of EL1. The electron source illuminates a square aperture which acts as the object for demagnification, unlike SEM-type round-beam systems where the Gaussian gun crossover is demagnified. This square-spot shaping aperture is at the center of the condenser lens (Köhler illumination). The condenser images the electron source (widely spaced shading) 1:1 into the entrance pupil defined by the beam-shaping round aperture in the demagnification section. The two demagnification lenses have the dual function of generating a 200:1 reduced image of the square aperture (narrow shading) and projecting the entrance pupil, with the truncated image of the Gaussian

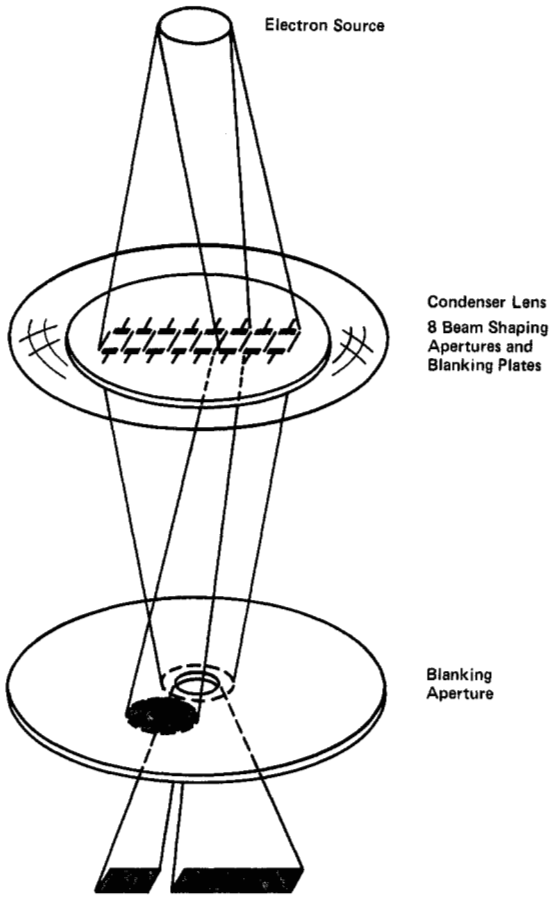

Fig. 3. Multibeam Schlieren technique.

crossover, into the center of the projection lens, accurately limiting the final beam semiangle. The reduced image of the square aperture is projected 1:1 into the target plane. The projection lens provides the working distance for the deflection yoke centered in the pole piece gap for minimum object-image distance. The pattern is written by moving the shaped beam in discrete jumps across the deflection field.

Other fixed-shape-beam arrangements have been reported by Trotel [21] and Varnell [22], the latter describing a round-beam shaping aperture using critical illumination for better definition of the source image at the target plane. The throughput in this case is less than that described for the square-shaped beam.

C. Multibeam

The multibeam system produces several identical shaped beams in parallel. Fig. 3 shows the basic imaging concept. The electron source illuminates an array of eight square shaping apertures equipped with individual blanking plates. The condenser forms a single source image superimposing all eight unblanked beams in the place of the blanking aperture, which acts as an entrance pupil for the subsequent demagnification and projection stages (see Section III-B). The intensity of individual beams is modulated by electrostatic fields which deflect the source image of the beam to be blanked (shaded trace) off the aperture. Analogous to Topler's Schlieren optics [23], slight changes in beam direction caused by variations in refractive index of otherwise transparent objects are thus transformed into amplitude contrast. The variations in refractive index are here imposed by the localized electrostatic fields. To avoid interference between adjacent beams, the field lines of the individual deflection units are well shielded and physically separated. Fig. 4 shows a schematic of our multibeam deflector.

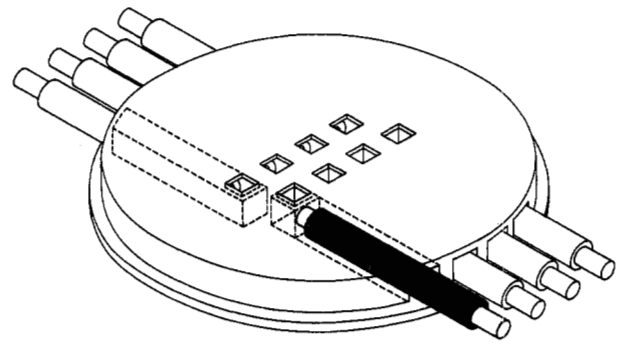

Fig. 4. Multibeam deflector eight-beam aperture plate with blanking electrodes.

The aperture plate forms two groups of four square beams each. The blanking signals are applied through electrodes in grounded channels. The entire unit is part of a heated aperture assembly and operates at about 300°C. The electrode material is aluminum and the insulation Al_2O_3 formed by anodizing. Electrodes and insulation are well shielded from the beams. The aperture pattern is demagnified and scanned across the target as a row of eight beams with a two-spot phase shift between the first group of four beams and the second.

A four-beam system was recently reported by Bell Laboratories [24] which, however, uses the dual-aperture approach (see Section III-D) with a more complex second aperture. The four-beam approach has been used in a raster-scan mode as a scheme to upgrade Bell Laboratories' EBES system.

Both multibeam approaches have in common that beam deflection can only be carried out collectively. The relative position of the individual beams cannot be varied and, therefore, cannot account for windage and design grid variations without tradeoffs in exposure efficiency.

D. Variable-Shaped Beam

The concept of variable spot shaping (VSS) received considerable attention since four independent research groups reported on the subject at the Palo Alto conference in 1977 [19], [24]-[26]. This paper primarily describes IBM's contribution.

Fig. 5 illustrates the basic VSS method. Two square apertures shape the beam spot. The image of the first square aperture, which appears in the plane of the second square aperture, can be shifted laterally with respect to the second aperture. A particular fraction of the total beam, which depends on the signal applied to the electrostatic shaping deflectors, passes through both apertures. The compound image formed by both apertures is subsequently demagnified and projected on the target.

A great variety of shapes can be generated at the switching speed of the shaping deflector electronics. For maximum

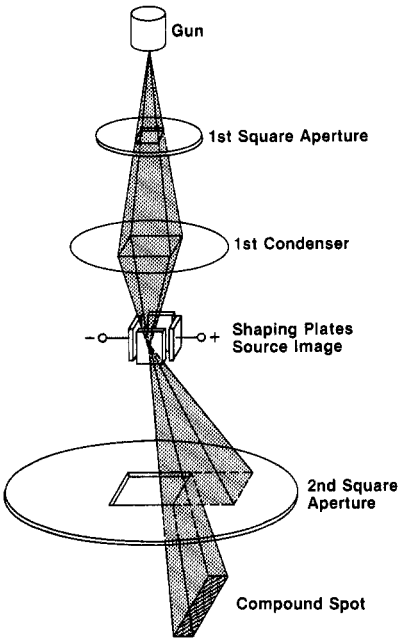

Fig. 5. Dual-aperture shaping method.

spot size, the image of the first aperture, identical in size and shape with that of the second one, would remain undeflected and would coincide with the second aperture. Alignment servos maintain their relative positions. Both apertures, as well as the shaping deflectors, can be mechanically rotated to compensate for image rotation of the condenser and the following magnetic lenses. The apertures are heated to prevent contamination.

The key to the VSS method is the optical separation of source and object images, described as the linked-beam trace [27].

The image formation of the two square-aperture objects can be manipulated without affecting the image formation of the source, which controls illumination and current density at the target as well as projection and deflection aberrations. In electron-beam lithography, variations in spot size must not change the current density of the remaining spot at the target, and spot edges must retain resolution and position. Fig. 6 shows the linked-beam trace for variable-spot shaping, which meets these requirements.

The electron source illuminates the first square aperture placed between source and first condenser. The first condenser performs the two functions of imaging this first square aperture onto the second square aperture and projecting the image of the source into the center of the spot-shaping deflector.

By placing the electrostatic shaping deflector symmetrically around the source image, the image of one object (first square aperture) can be shifted relative to the other object (second square aperture) without affecting the position of subsequent source images. Despite substantial beam shift at the second square aperture, there is no beam movement at the round third aperture, which controls illumination and resolution.

The functions after the second condenser lens—e.g., blanking, demagnification, spot deflection, and dynamic corrections for field curvature and deflection astigmatism—remain unaffected by variation in spot shape. The beam position remains unchanged within the final lens; consequently, the delicate balance of aberrations is maintained, except for those due to interactions. Image blurring resulting from Coulomb interactions between beam electrons is a function of total beam current. Variations in spot size and the corresponding beam current cause interaction aberrations to vary. The design of variable-shaped-spot systems with high total beam currents must, therefore, minimize interaction effects.

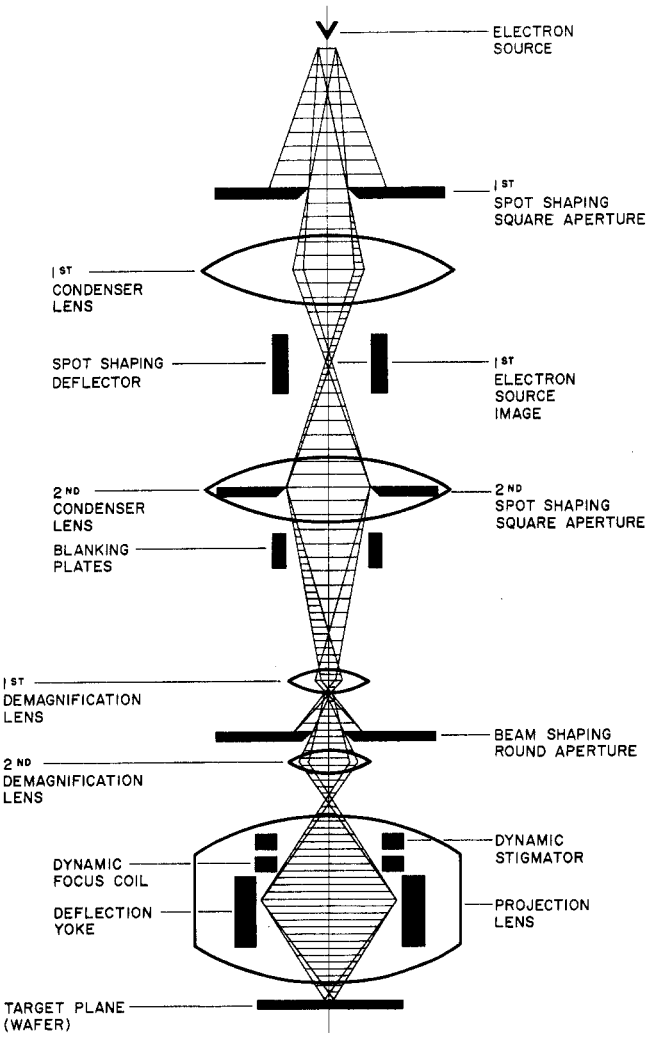

Fig. 6. Linked-beam trace for variable-spot shaping.

Corrections for proximity effects which require windage (linewidth variation) and/or dose variations for particular pattern features can be applied conveniently in VSS systems. It has been demonstrated that in SEM-type systems proximity effects can be adequately corrected by varying the dose of so-called "primitive shapes" [28] rather than on a spot-by-spot basis. These primitive shapes are normally at least the size of a VSS exposure. For a small percentage of very critical shapes, it may be advantageous to partition individual spot shapes further at an insignificant penalty in throughput.

E. Character Projection

Character projection is our extension of the dual-aperture VSS technique where the second aperture is replaced by a

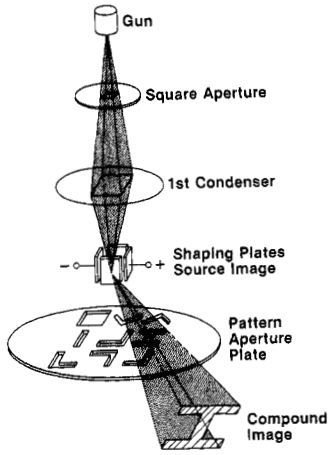

Fig. 7. Character aperture shaping method.

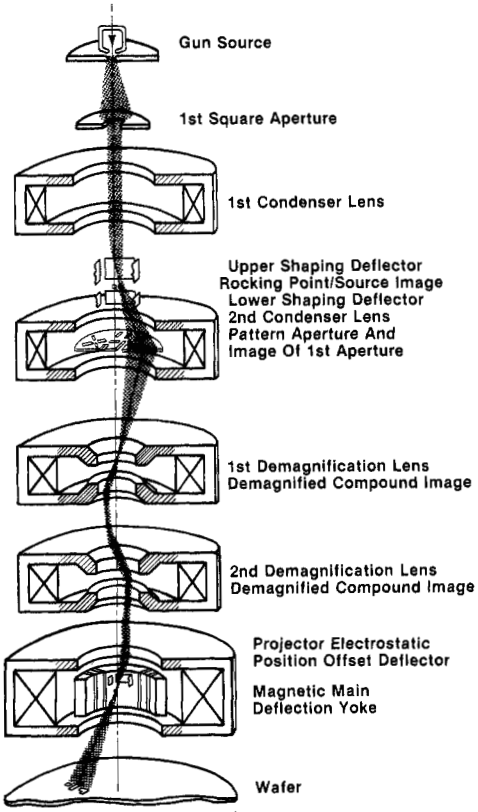

Fig. 8. Schematic of character projection column.

character plate with an array of complex aperture shapes (characters) as shown in Fig. 7 [20]. These can be selected in full or in part to compose and project pattern cells with up to 1600 image points. Nonrectilinear and curved patterns can easily be included.

Fig. 8 shows the arrangement of the electron-optical column and the image formation. It is a five-lens system designed as an electron-optical bench of modular components.

The electron source illuminates the first square aperture which acts as one object for demagnification and projection. The second object is the pattern aperture which contains the array of "character" shapes. The pattern aperture is variably illuminated with the image of the first aperture. However,

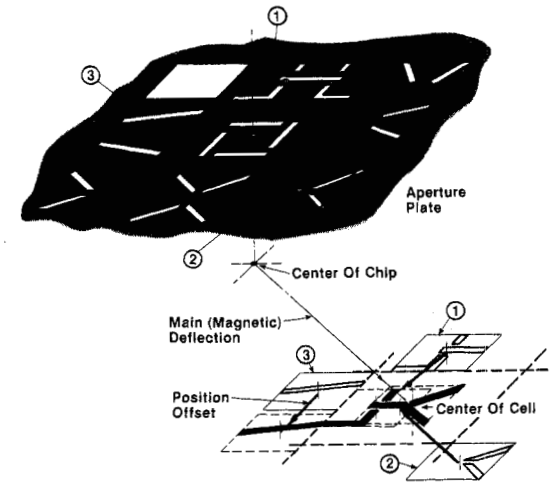

Fig. 9. Principle of pattern selection, projection, and offset correction.

the pattern aperture is 25 times larger than the square first aperture. Köhler's illumination principle is used to separate the source image from the object images. The first condenser performs the dual function of imaging the first square aperture onto the plane of the pattern aperture; it projects the image of the source into the center of the spot-shaping deflector. The spot-shaping deflector permits placement of the first-aperture image at any character or portion of any character shape. Subsequently, demagnification lenses project that character or portion onto the target. The second condenser controls the illumination projecting the source image into the entrance pupil of the two-stage demagnification and the projection section. The placement of the composite image at the target is performed by a main magnetic deflection yoke located inside the projection lens [2], and an electrostatic pattern offset. Fig. 9 shows an example of an aperture plate actually used. The composition of a pattern using three shapes from the aperture plate is indicated. The position of any selected shape projected on the wafer with respect to the cell center is dictated by its position on the aperture plate. This is indicated by the open shapes ①, ②, ③ in Fig. 9. In order to move these shapes into their nominal position (shown solid in Fig. 9) the position offset must be corrected by an auxiliary (electrostatic) deflection superimposed on the main deflection. The exposure of each shape within a given cell is defined by a set of data describing the shaping in X and Y directions, the position offset correction in X and Y directions, and if necessary, the exposure time to correct for proximity effects.

In the design of the aperture plates two points have been considered in particular. Firstly, enough area had to be provided around each character to avoid interference with an adjacent character when any desired portion of one character is selected; secondly, stitching of patterns on the target was confined to noncritical areas avoiding placement errors that would impact circuit functions. In case of a T and I bar bubble memory pattern, for instance, the character boundary will not be placed inside the gap region, which is critical for bubble propagation, but in areas outside (see Fig. 20). Character projection reduces the total amount of data required to write a pattern. Maintaining the data-rate and deflection

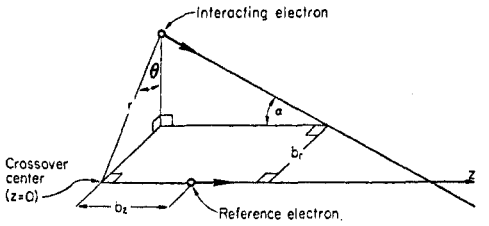

Fig. 10. Interaction mechanism.

speed, throughput can be increased by reducing the time to expose a field, or maintaining the throughput, the data-rate, deflection speed, or beam current can be reduced, resulting in higher resolution and/or less costly data-processing equipment. Apertures have also been designed for nonrectilinear and for curved shapes, which greatly extend the flexibility of shaped-beam lithography.

IV. Limitations

The previous section on beam shaping may suggest there is no limit to the enhancement of exposure efficiency. There are, however, some inherent limitations.

The exposure speed enhancement of shaped beams is based on the fact that a shaped beam can carry orders of magnitude more current than the equivalent Gaussian round beam without increasing classical first- and third-order aberrations. However, Coulomb forces between beam electrons increase with higher currents. The key limitation of shaped-beam systems is, therefore, inherent in the particle character of the electrons and their stochastic interactions [29]. Fig. 10 illustrates the basic interaction mechanism [30].

On a reference electron moving along the beam axis in the z direction, the force

$$F = \frac{K(b_r, \alpha z, b^2)}{[b^2 + (\alpha z - r\cos\Theta)^2]^{3/2}} \tag{1}$$

with

$$K = \frac{e_0 2}{4\pi\epsilon_0} \quad \text{and} \quad b^2 = b_r^2 + b_z^2$$

is exerted by another electron with angle α to the beam axis, impact parameter b, trajectory distance r from the axis in the crossover plane ($z = 0$), and angle Θ between r and b_r.

The angular and trajectory displacements cause aberrations in the form of image blurring. In the design optimization of a shaped-beam system, this image blurring has to be included together with first- and third-order aberrations.

It should be noted, however, that for variable-shape beams with their dramatically changing beam currents, one additional interaction effect becomes significant: space-charge diversion. For fixed-beam currents, space-charge diversion is not detectable because the defocussing effect is compensated by a slight increase of the projection lens focal power. Unlike the individual stochastic Coulomb interaction of beam electrons, space-charge diversion is a correctable effect caused by the "eigen" charge of the beam. For variable-shape beams with their rapidly (<20 ns) changing eigen charge, a defocussing

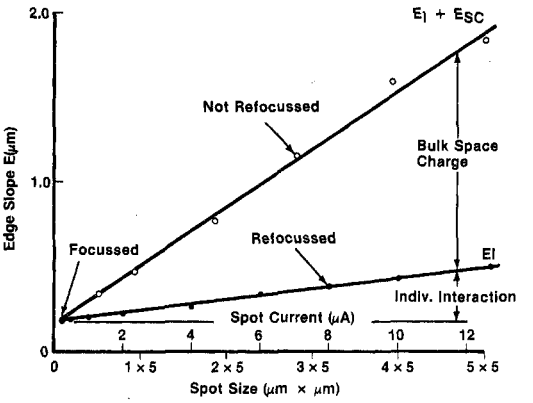

Fig. 11. Space-charge and individual electron interaction effects on the edge slope of variable shaped spot.

results if not corrected by an equally fast dynamic focus lens. Fig. 11 shows the effect of space charge and individual interaction on the edge slope on a variable-shape beam—with and without refocussing.

V. Deflection Concepts

The electron-optical performance of scanning lithography systems and in particular the number of resolved lines per field depend in great part on the deflection concept used. To cover a full chip at high resolution without stitching fields together requires typically a deflection system capable of producing several thousand fabricated lines per field. Fig. 12 shows schematically the various concepts used.

Table I compares their electron-optical performance data for two distinctly different applications: (A) the low-current, Gaussian round beam, and (B) the high-current, shaped beam. In both cases, third-order aberrations after dynamic correction for field curvature and deflection astigmatism are listed together with chromatic aberration.

The force of the Coulomb scattering events can cause significant changes in momentum and velocity along the electron beam. The force component in the z direction leads to energy changes known as the Boersch effect [31]. The thermal energy spread of the beam electrons which is typically a few tenths of a volt can be increased by more than an order of magnitude. The Coulomb interaction will ultimately determine the maximum current that can be focussed onto a shaped beam.

This effect can result in substantial chromatic aberrations as the beam passes through focussing and deflection elements [32].

Following Loeffler and Hudgin [33] the three components of Coulomb forces generate angular changes and displacements of the electron trajectories, $\Delta\alpha$ and Δr, respectively, in addition to energy changes ΔE

$$\Delta E \propto \frac{1}{\alpha r}\,\Omega(\lambda r)$$

$$\Delta\alpha \propto \frac{1}{V_r}\,\Lambda(\lambda r)$$

$$\Delta r \propto \frac{1}{V\alpha^2}\,\Gamma(\lambda\alpha L) \tag{2}$$

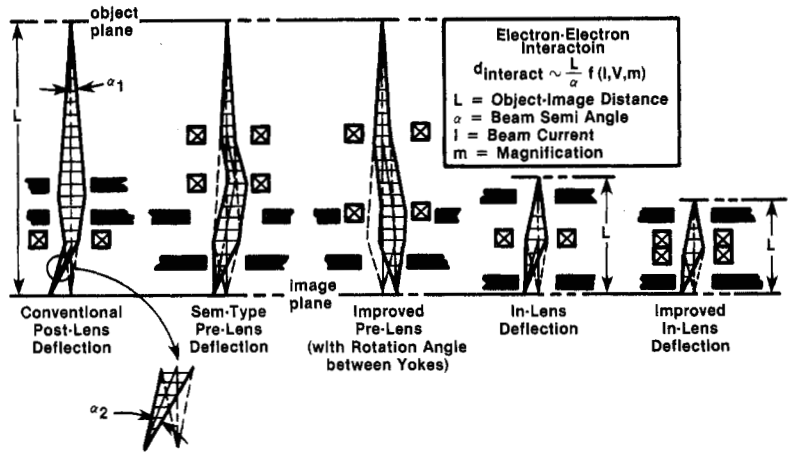

Fig. 12. Deflection concepts of scanning-electron-beam systems.

TABLE I
COMPARISON OF IMAGING AND DEFLECTION SYSTEMS

(A) 0.25-μm ROUND SPOT (B) 2.5-μm SQUARE SPOT	CONVENTIONAL POST-LENS DEFLECTION		CONVENTIONAL SEM PRE-LENS DEFLECTION		IMPROVED PRE-LENS DEFLECTION		IN-LENS DEFLECTION		IMPROVED IN-LENS DFFLECTION	
	(A)	(B)	(A)	(B)	(A)	(B)	(A)	(B)	(A)	(B)
SEMI-ANGLE α (mr)	5.0	7.5	5.0	7.5	5.0	7.5	5.0	7.5	5.0	7.5
ENERGY SPREAD ΔE (eV)	2.5	7.5	2.5	7.5	2.5	7.5	2.5	7.5	2.5	7.5
BEAM CURRENT I (μA)	0.025	3.0	0.025	3.0	0.025	3.0	0.025	3.0	0.025	3.0
ABERRATIONS (μm) (CORNER OF 5X5mm FIELD)										
THIRD ORDER AFTER CORRECTIONS	0.23	0.24	0.47	0.48	0.14	0.15	0.13	0.13	0.05	0.07
TRANSVERSE AND AXIAL CHROMATIC	0.27	0.78	0.31	0.81	0.03	0.09	0.13	0.41	0.07	0.22
INTERACTION	0.00	0.78	0.00	0.78	0.00	0.78	0.00	0.28	0.00	0.18
TOTAL AFTER CORRECTION	0.35	1.12	0.56	1.22	0.15	0.80	0.19	0.51	0.09	0.29

where a is the beam semiangle, r the crossover of probe radius, V the acceleration potential, and L, G, Q, are the dimensionless functions of the axial electron density of the beam, and r, or a and L, the beam length.

The more complex situation of a multibeam arrangement requires some refinement of the analytical treatment. The beams are physically separated in the vicinity of the object and its image planes, overlap, however, in the vicinity of the source image planes. Experimental results indicate the same basic trends as for single shaped beams with some modification in interaction amplitude which can be expressed through an effective beam semiangle

$$\alpha_{\text{eff}} = G\alpha \tag{3}$$

where G is a function of the multibeam pattern geometry.

In case (A), based on a comparison published by Munro [34], the use of an LaB_6 gun is assumed with its lower energy spread [35] and its high brightness concentrated in a narrow emission cone [36]. For case (B) a tungsten gun, though limited in brightness and burdened with higher energy spread, is used because it illuminates the shaped spot more uniformly. The most striking difference between the two applications is the interaction.

While totally negligible in the low-current case, interaction aberrations represent a dominant limitation for high-current shaped beams. Only the more recently developed in-lens deflection schemes [37]-[39] minimize interactions causing image blurring. At first, approximation shows that image blurring is proportional to the object image distance L and inversely proportional to the beam semiangle

$$d \propto \frac{L}{\alpha}(I, V, M). \tag{4}$$

The modifying parameters are beam current I, acceleration potential, and magnification. Trajectory displacement reaches a minimum for a magnification close to unity and a foreshortened distance between object and image plane [31]. Both criteria favor a compact arrangement of projection lens and deflection yoke. The two in-lens deflection arrangements meet that requirement. Superimposing projection and deflection makes it possible to compensate lens and yoke aberrations in addition to reducing Coulomb interactions.

Fig. 13 illustrates the compensation of the isotropic and nonisotropic chromatic deflection aberrations. A single isolated yoke deflects electrons of lower energy further than those of higher energy. Placing the yoke inside a lens com-

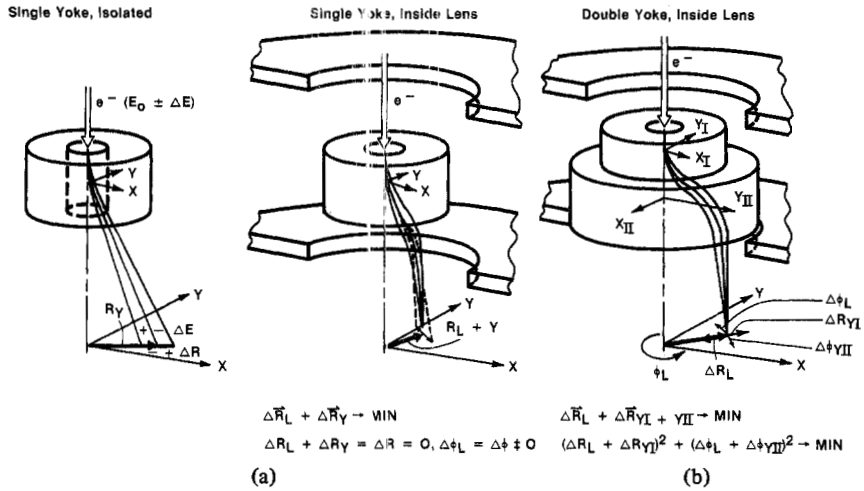

Fig. 13. Compensation of chromatic deflection aberrations.

pensates this dispersion RY with the opposed isotropic dispersion of the lens RL. The radial component of the chromatic aberration can, therefore, be totally eliminated [17]. What remains is the nonisotropic chromatic aberration of the magnetic lens caused by image rotation.

Adding a second yoke rotated "against" the image rotation of the lens permits compensation of the nonisotropic chromatic aberration of the lens as well [40]. The compensation effects have been experimentally verified [39]. The data shown in Table I for the in-lens arrangements reflect the practical results. The technique of field stitching is a different approach to the deflection problem. Here the deflection field is restricted to an area smaller than a chip in which the aberrations are still tolerable. The small fields are then stitched together using registration marks [41] or the relative position of beam and wafer are tracked with laser interferometers [42].

The EBES system [43] combines small-field deflection with a continually moving table for more efficient exposure.

VI. Results

The performance of shaped-beam systems can be demonstrated in the form of resist exposures and through the display of current density profiles of the beam spot in the target plane. The conventional SEM video display of topographic target details will not reveal the resolution of a shaped-beam system since the image contrast in the SEM is determined by the size of the beam spot rather than its edge slope. Fig. 14 shows the beam current profile of a shaped beam in one lateral dimension. This profile is obtained by scanning the focussed spot with constant velocity across a straight wire and by differentiating the signal produced by a detector measuring the integral beam current in transmission. The signal representing the integral beam current is shown in the upper trace while the lower trace shows the differentiated signal representing the current density profile, laterally expanded 5X with respect to the upper trace. A Faraday cup is used to calibrate the signal amplitude. The diameter of the wire is used to calibrate the spot size, which is defined as the pulsewidth at

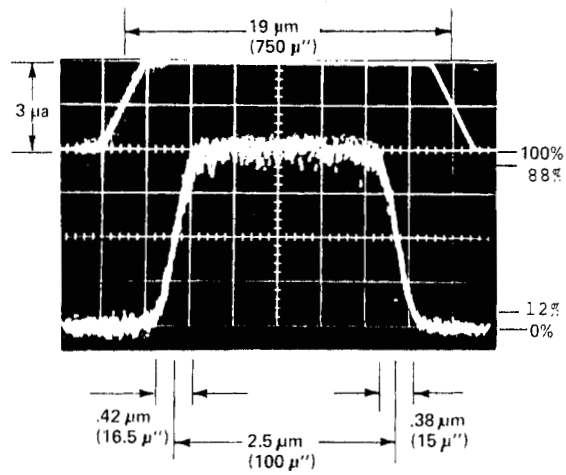

Fig. 14. Current density profile of fixed-shape spot.

half amplitude. Resolution is defined as the half-width of the second derivative, which is equivalent to the lateral edge-slope projection of the first derivative between 12- and 88-percent points of the pulse amplitude. The signal amplitude corresponds to the current density of the spot and is calibrated for a given width orthogonal to the scan direction.

In a successful implementation of a variable-spot-shaping method, variations in spot size must have no effect, anywhere in the field of deflection, on current density of the remaining spot, on edge resolution, or on placement of unaffected spot edges. The following oscilloscope traces and SEM micrographs demonstrate that these requirements are met. Fig. 15 shows four different shaping conditions for the dual-aperture method.

In the case of the nominal spot, the image of the first square aperture (cross hatched) coincides with the opening in the second aperture (shaded) to generate a square spot of maximum size at the target. The following positions represent shape variations in either direction or both simultaneously, to generate rectangles and squares as indicated.

Corresponding beam current profiles in the X and Y directions are shown in Fig. 16. All four spot shapes were dis-

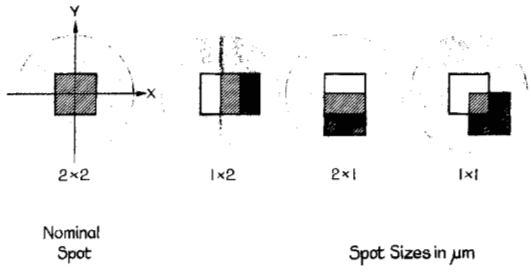

Fig. 15. Dual-aperture shape variation.

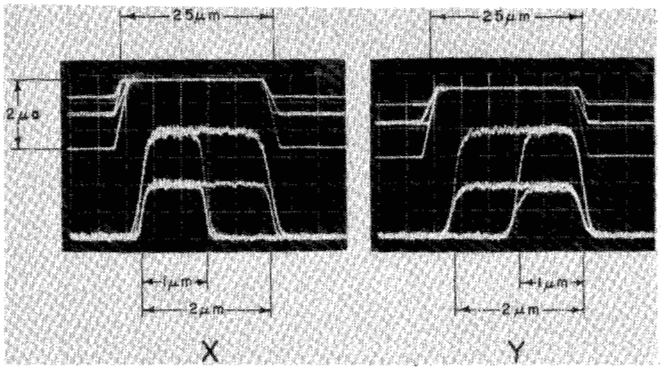

Fig. 16. Variable spot shaping: super-imposed current density profiles in X and Y direction for the four different shapes in Fig. 15.

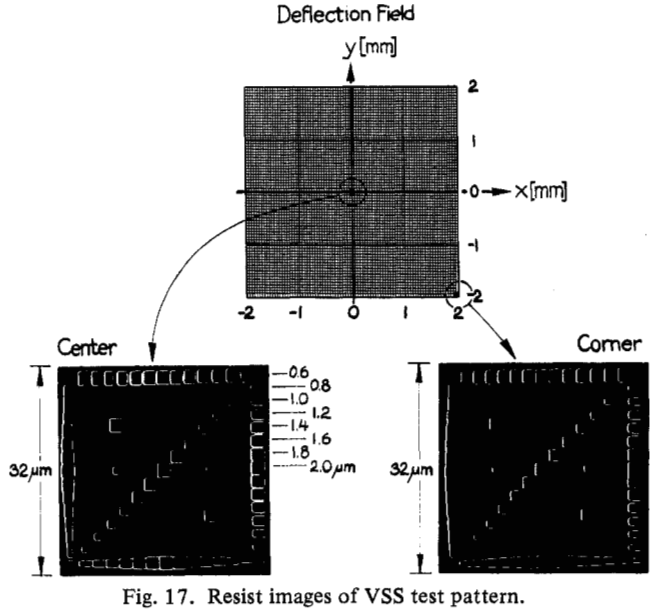

Fig. 17. Resist images of VSS test pattern.

played stroboscopically at high switching speed and superimposed. Shape variations in the scanning direction result in pulsewidth variations of the derivative signal at constant amplitude. The rate of current change is unaffected; the duration of the signal transition, however, is altered.

Shape variations orthogonal to the scan direction result in pulse-height variations at constant width. The duration of the signal transition of the upper trace remains constant; however, the change in beam current causes the slope of the transition to change. The reduction in pulse amplitude of the derivative signal is not to be interpreted as showing a loss of current density. The 50-percent reduction in amplitude corresponds to a 50-percent size reduction orthogonal to the scan.

The superimposed signals shown in Fig. 16 demonstrate

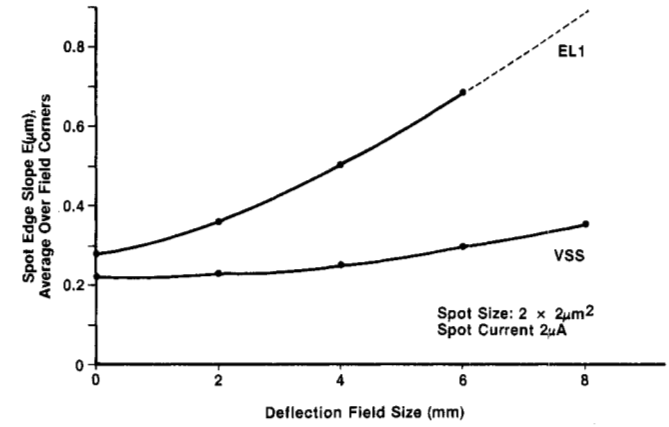

Fig. 18. Spot edge slope as a function of deflection field size for EL1 and VSS systems.

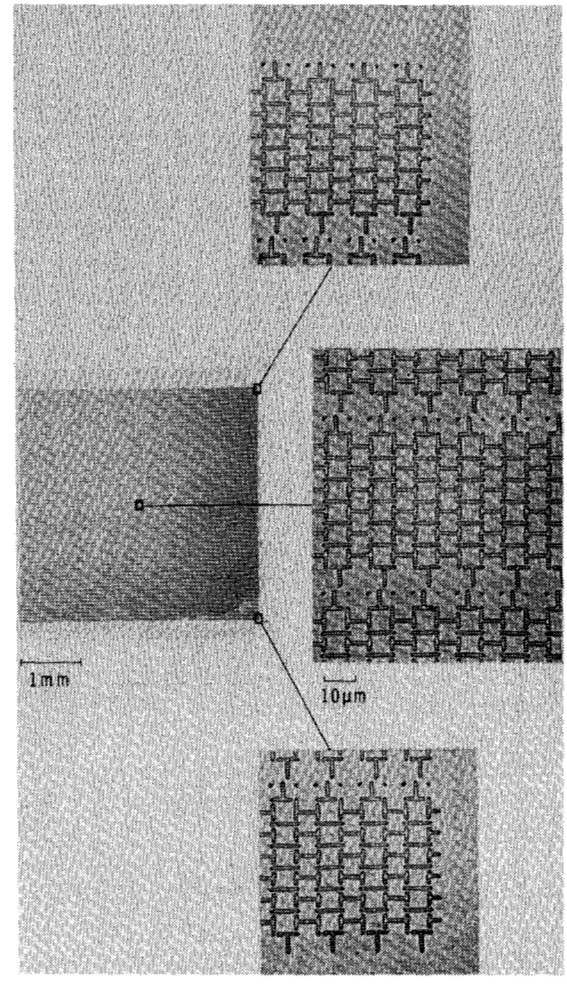

Fig. 19. Racetrack pattern for magnetic-bubble propagation exposed by character projection technique.

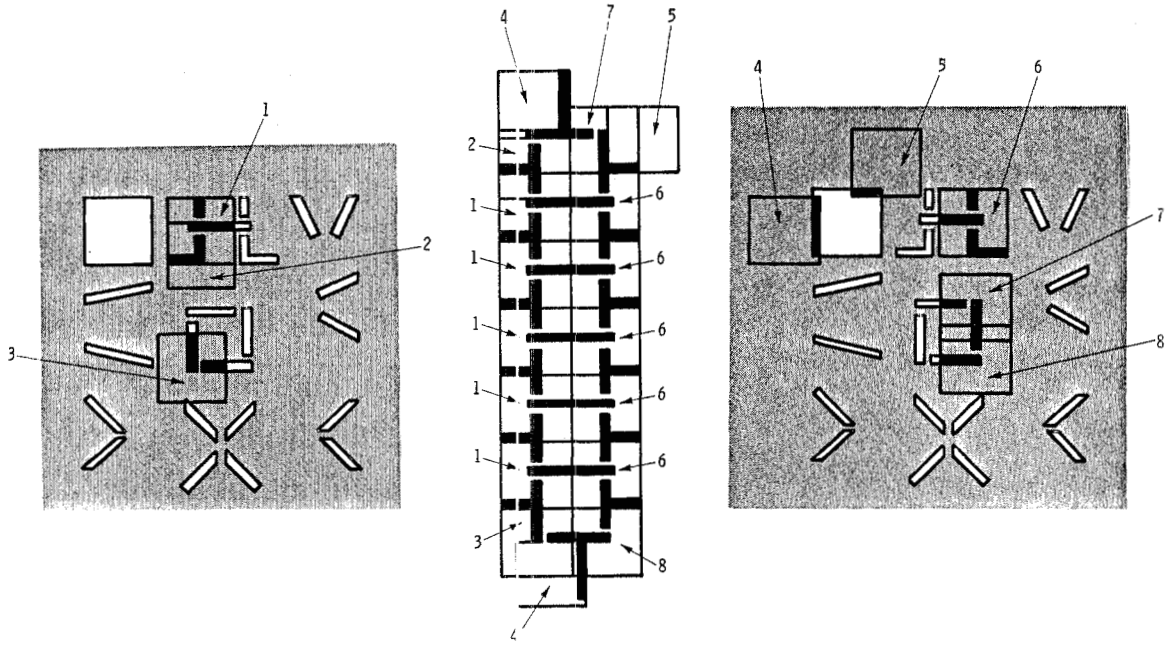

Fig. 20. Character compositions of short race track.

that current density remains constant for different spot shapes, and that unchanged spot edges maintain position and resolution within the accuracy of the measurement (0.1 μm). To check for positional stability, the 50-percent points of all amplitudes have to be compared.

Fig. 17 shows two SEM micrographs of resist images exposed by the VSS method at a beam current density of 50 A/cm^2. The basic pattern cell of 16 X 16 nominal spot positions, which contains shapes from 0.6 X 0.6 up to 2 X 2 μm is repeated 125 X 125 times over the 4 X 4-mm deflection field. Pattern fidelity and resolution are maintained for both the center and the corner positions of the deflection field. The test exposures demonstrate that VSS functioned properly with a deflection capability of over 5000 fabricated lines per field.

The pattern in Fig. 17 was obtained using the improved in-lens deflection method with yokes in the pole piece gap of the projection lens. The extent of the improvement in deflection of the VSS system over EL1 is illustrated in Fig. 18, which shows spot edge slope measurements for the two systems [39].

A pattern generated with the character projection technique is shown in Fig. 19 [20]. Sixteen thousand (16 000) short racetracks were exposed on a garnet wafer with a total of 3 X 10^5 flashes in a few tenths of a second. The micrographs show 1-μm T and I bars with 0.75-μm gaps over a field of 4 X 4 mm. There is no difference in image quality between the center and corners of the chip. The stitching of character, shapes occurs in noncritical areas outside the gap region (Fig. 20). Magnetic bubbles were successfully propagated on all locations of the chip.

Fig. 21 shows three of IBM's EL1 systems in a production line. The electron-beam columns are mounted on large vacuum chambers which house the mechanical wafer stage. Each system is supported by a vibration isolation table. To the left of the table is the wafer preparation station which automatically loads and unloads wafers in and out of the vacuum chambers.

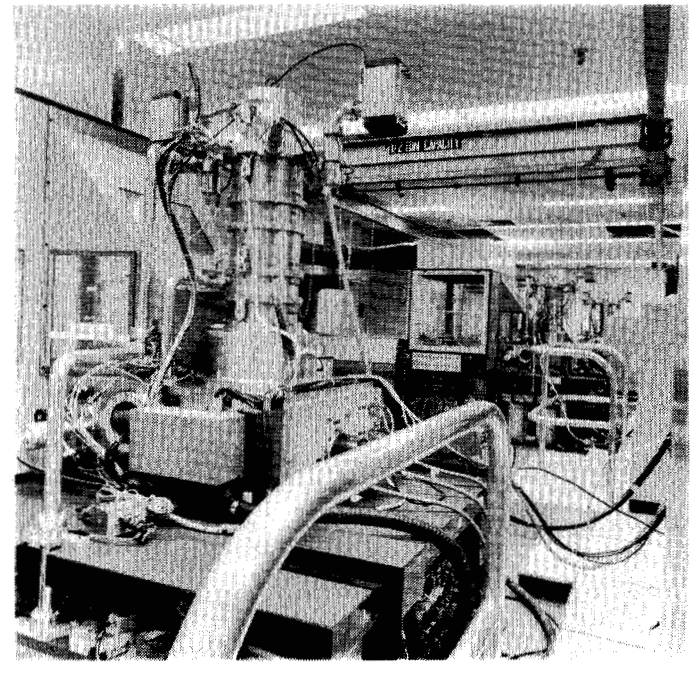

Fig. 21. EL1 systems in production line.

Fig. 22 shows a typical logic chip fabricated using EL1 for personalization of the first-level metal, vias, and second-level metal. The chip measures 4.6 mm on each side and contains more than 700 transistor–transistor circuits. The electron-beam registration marks are visible in the four corners. Fig. 23 is an area enlargement of the above chip showing in more detail the first-level metal (horizontal lines) second-level metal (vertical lines), and the connecting vias (circular shapes).

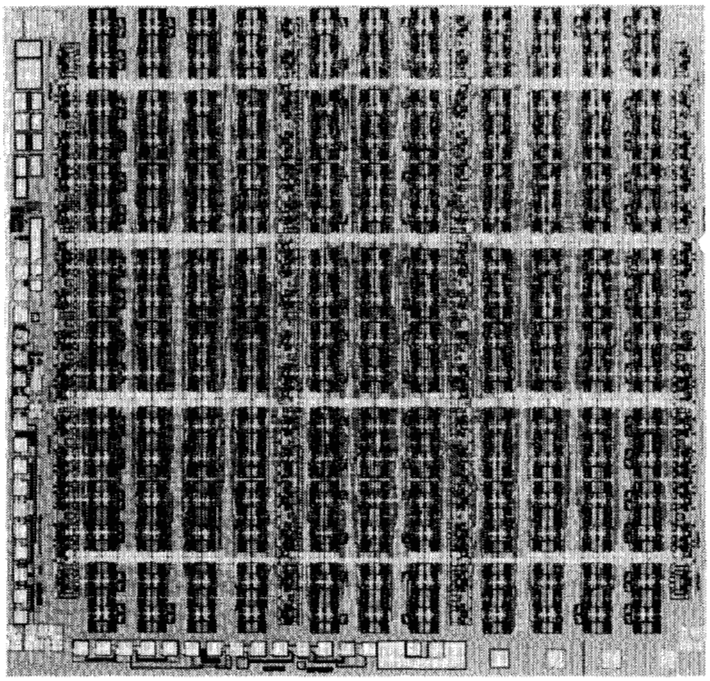

Fig. 22. Bipolar chip fabricated using EL1. Chip measures 4.6 mm on each side.

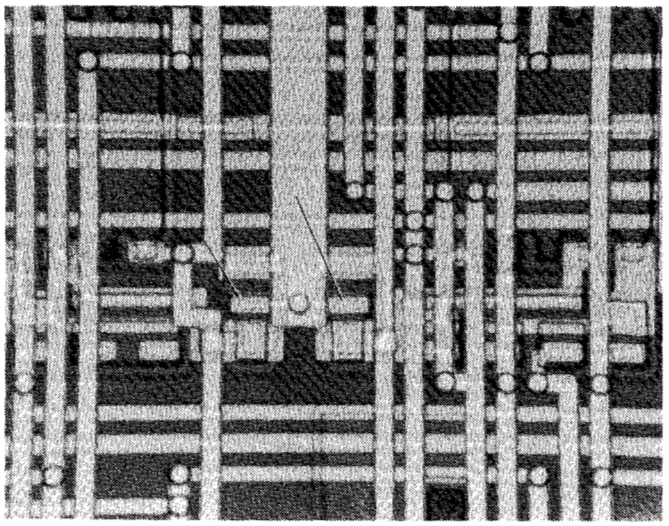

Fig. 23. Detail of chip in Fig. 22. Arrows point to 2.5-μm wide contact holes.

The arrows point to contact holes of 2.5-μm width. Maximum throughput is 22, $2\frac{1}{4}$-in wafers/h. The availability of the EL1 systems over a period of several years average more than 85 percent [44].

References

[1] R. F. M. Thornley and M. Hatzakis, "Electron optical fabrication of solid-state devices," in *Rec. 9th Symp. Electron, Ion, and Laser Beam Technol.* San Francisco, CA: San Francisco Press, 1967, p. 94.

[2] M. Hatzakis and A. N. Broers, "High resolution electron-beam fabrication," in *Rec. 10th Symp. Electron, Ion, and Laser Beam Technol.* San Francisco, CA: San Francisco Press, 1969, p. 107.

[3] T. H. P. Chang, "Device fabrication using a scanning electron beam system," in *4th Ann. SEM Symp. (IITRI)*, p. 417, 1971.

[4] F. S. Ozdemir, E. D. Wolf, and C. R. Buckey, "Computer-controlled SEM system for high resolution micro-electronic pattern fabrication," in *Rec. 11th Symp. Electron, Ion, and Laser Beam Technol.* San Francisco, CA: San Francisco Press, 1971, p. 463.

[5] G. L. Varnell, D. F. Spicer, and A. C. Rodger, "E-beam writing techniques for semiconductor device fabrication," *J. Vac. Sci. Technol.*, vol. 10, no. 6, p. 1048, 1973.

[6] H. N. Yu, R. H. Dennard, T. H. P. Chang, C. M. Osburn, V. Dionardo, and H. E. Luhn, "Fabrication of a miniature 8k-bit memory chip using electron beam exposure," *J. Vac. Sci. Technol.*, vol. 12, no. 6, p. 1297, 1975.

[7] T. H. P. Chang, A. D. Wilson, A. J. Speth, and C. H. Ting, "Vector scan 1: An automated electron beam system for high resolution lithography," in *Proc. Symp. Electron and Ion Beam Science and Technology*, p. 392, 1976.

[8] S. A. Evans, J. L. Bartelt, B. J. Sloan, and G. L. Varnell, "Fabrication of integrated injection logic using e-beam lithography," *J. Vac. Sci. Technol.*, vol. 15, no. 3, p. 969, 1978.

[9] A. N. Broers, J. Cuomo, J. Harper, W. Molzen, R. Laibowitz, and M. Pomerants, "High resolution electron beam fabrication using STEM," in *9th Internat. Conf. on Electron Microscopy* (Toronto, Canada), p. 343, 1978.

[10] P. R. Malmberg, T. W. O'Keefe, and M. M. Sopira, "LSI pattern generation and replication by electron beams," *J. Vac. Sci. Technol.*, vol. 10, p. 1025, 1975.

[11] J. P. Scott, "Electron image projector," in *Proc. 6th Int. Conf. on Electron and Ion Beam Sci. and Technol.* R. Bakish, Ed. (Electrochem. Soc. Princeton, NJ), p. 123, 1974.

[12] H. Koops, G. Möllenstedt, and R. Speidel, "Zur Eleletronenoptischen Microminiaturisation von Schablonen," *Optik*, vol. 28, p. 518, 1968.

[13] M. B. Heritage, "Electron-projection micro-fabrication system," *J. Vac. Sci. Technol.*, vol. 12, p. 1135, 1975.

[14] R. Speidel and M. Mayr, "Electron beam projection system with photocathodes," *Optik*, vol. 48, p. 247, 1977.

[15] E. V. Weber and H. S. Yourke, "Scanning electron beam system turns out IC wafers fast," *Electron.*, vol. 50, no. 23, p. 96, 1977.

[16] H. C. Pfeiffer and K. H. Loeffler, "A high current square spot probe for micro pattern generation," in *7th Int. Conf. on Electron Microscopy* (Grenoble, France), p. 63, 1970.

[17] H. C. Pfeiffer, "New imaging and deflection concept for probe-forming microfabrication systems," *J. Vac. Sci. Technol.*, vol. 12, no. 6, p. 1170, 1975.

[18] —, "Beam shaping techniques in scanning electron lithography systems," in *9th Int. Conf. on Electron Microscopy* (Toronto, Canada), vol. 1, p. 162, 1978.

[19] —, "Variable spot shaping for electron-beam lithography," *J. Vac. Sci. Technol.*, vol. 15, no. 3, p. 887, 1978.

[20] H. C. Pfeiffer and G. O. Langner, "Advanced beam shaping techniques for electron lithography," in *Extended Abstracts of 8th Int. Conf. on Electron and Ion Beam Sci. and Technol.* (Seattle, WA). Electrochem. Soc., Princeton, NJ, p. 893, 1978.

[21] J. Trotel, "Electrocomposers, a fast electron beam pattern generator," in *Proc. 6th Int. Conf. on Electron and Ion Beam Sci. and Technol.*, R. Bakish, Ed. (Electrochem. Soc. Princeton, NJ), p. 325, 1976.

[22] G. L. Varnell, D. F. Spicer, A. C. Rodger, and R. D. Holland, "High speed electron beam pattern generation," in *6th Int. Conf. on Electron and Ion Beam Sci. and Technol.*, R. Bakish, Ed. (Electrochem. Soc. Princeton, NJ), p. 97, 1974.

[23] A. Töpler, *Poggendorff's Annalen*, vol. 131, p. 180, 1867.

[24] M. G. R. Thomson, R. J. Collier, and D. R. Herriott, "Double-aperture method of producing variable shaped writing spots for electron lithography," *J. Vac. Sci. Technol.*, vol. 15, no. 3, p. 891, 1978.

[25] E. Goto, T. Soma, and M. Idesawa, "Design of a variable-aperture projection and scanning system for electron beam," *J. Vac. Sci. Technol.*, vol. 15, no. 3, p. 883, 1978.

[26] J. Trotel, "Dynamic beam shaping," *J. Vac. Sci. Technol.*, vol. 15, no. 3, p. 872, 1978.

[27] A. Köhler and Z. Wiss, *Microscopie*, vol. 10, p. 433, 1893.

[28] M. Parikh, "Self-consistent proximity effect correction technique for resist exposure (SPECTRE)," *J. Vac. Sci. Technol.*, vol. 15, no. 3, p. 931, 1978.

[29] H. C. Pfeiffer, "Basic limitations of probe forming systems due to electron-electron interaction," in *Proc. 5th Ann. SEM Symp. (IITRI)*, p. 113, 1972.

[30] K. H. Loeffler, "Energy spread generation in electron-optical instruments," *Z. Agnew. Phys.*, vol. 27, p. 145, 1969.
[31] H. Boersch, "Experimentelle Bestimmung der Energieverteilung in Thermisch Ausgelösten Elektronen Strahlen," *Z. Phys.*, vol. 139, p. 115, 1954.
[32] J. L. Mauer, H. C. Pfeiffer, and W. Stickel, "Electron optics of an electron-beam lithographic system," *IBM J. Res. Develop.*, vol. 21, no. 6, p. 515, 1977.
[33] K. H. Loeffler and R. H. Hudgin, "Energy-spread generation and image deterioration by the stochastic interactions between beam electrons," in *7th Int. Conf. on Electron Microscopy* (Grenoble, France), p. 67, 1970.
[34] E. Munro, "Design and optimization of magnetic lenses and deflection systems for electron beams," *J. Vac. Sci. Technol.*, vol. 12, no. 6, p. 1146, 1975.
[35] H. C. Pfeiffer, "Experimental investigation of energy broadening in electron optical instruments," in *Rec. 11th Symp. Electron, Ion, and Laser Beam Technol.* San Francisco, CA: San Francisco Press, 1971, p. 239.
[36] W. Stickel and H. C. Pfeiffer, "Emission characteristics of the LaB_6 electron gun," in *Proc. 12th Symp. Electron, Ion, and Laser Beam Technol.*, p. 415, 1973.
[37] H. C. Pfeiffer, "A new concept of superimposed deflection and projection for probe-forming electron beam systems," in *8th Int. Congr. on Electron Microscopy* (Canberra, Australia), p. 56, 1974.
[38] E. Munro, "Reducing deflection aberrations in electron-beam scanning systems," *IBM Tech. Disclosure Bull.*, vol. 17, p. 3107, 1975.
[39] W. Stickel and H. C. Pfeiffer, "Optics of a variable shaped electron beam column," in *Extend. Abstr. 8th Int. Conf. on Electron and Ion Beam Sci. and Technol.* (Seattle, WA). Princeton, NJ: Electrochem. Soc., p. 890, 1978.
[40] H. Ohiwa, E. Goto, and A. Ono, "Elimination of third-order aberrations in electron-beam scanning systems," *Electron. Commun. Japan*, vol. 54B, p. 44, 1971.
[41] A. D. Wilson, T. H. P. Chang, and A. Kern, "Experimental scanning electron-beam automatic registration system," *J. Vac. Sci. Technol.*, vol. 12, no. 6, p. 1240, 1975.
[42] O. Cahen, R. Sigille, and J. Trotel, "Automatic control of an electron beam pattern generator," in *Proc. 5th Int. Electron and Ion Beam Sci. and Technol.*, R. Bakish, Ed. (Electrochem. Soc. Princeton, NJ), p. 92, 1972.
[43] D. R. Herriott, R. J. Collier, D. S. Alles, and J. W. Stafford, "EBES: A practical electron lithography system," *IEEE Trans. Electron Devices*, vol. ED-22, p. 385, 1975.
[44] R. D. Moore, "Reliability, availability, and serviceability of direct wafer exposure electron beam systems," in *Proc. Int. Conf. on Microlithography* (Paris, France), p. 153, 1977.

Hans C. Pfeiffer received the B.S. degree in 1960, the M.S. degree in 1964, and the Ph.D. degree in 1967, all in physics and electron optics, from the Technical University in Berlin, Germany, as a student of Prof. H. Boersch.

He joined IBM in 1968 and since then pursued new electron optical concepts for advanced lithography systems. He developed IBM's first electron-beam columns with shaped beam (EL1) and variable shaped beam (EL2) for high-speed pattern exposure. He received several IBM awards for his patents and for outstanding contributions in the field of electron-beam technology. He is presently a Senior Engineer and Manager of the electron-beam technology team in IBM's East Fishkill Laboratory, Hopewell Junction, NY.